EPJ manuscript No.
(will be inserted by the editor)

A Phenomenological Solution to the Hubble and S_8 Tensions Based on Time-flow Evolution

Penghong Jiao[1]

Independent Researcher, Beijing 100010, China

Received: date / Accepted: date

Abstract. The ΛCDM model confronts two increasingly significant observational conflicts: the Hubble constant H_0 tension ($+8.3\%$, $> 5\sigma$) and the S_8 tension (-8.4%, $\sim 3\sigma$). The near-identical absolute magnitudes and opposite signs of these deviations suggest a common kinematic origin rather than modifications to the cosmic energy budget. We propose a phenomenological framework in which physical proper time τ is an emergent order parameter of energy flux from higher dimensions into the 3-dimensional observable space, satisfying $d\tau = a(t)^{-1}\, dt$. This yields a proper-time rate $\gamma(z) \equiv d\tau/dt = 1 + z$. Introducing a single empirical parameter Q calibrated by the observed H_0 tension, the model yields an effective late-time factor $\bar{\gamma}_{\rm late} \simeq 1.083$, from which the S_8 tension and $f\sigma_8$ suppression follow with no additional free parameters, driven by a dynamical competition between the constant thrust from Q and the standard ΛCDM Hubble drag. The same time-flow mechanism naturally suppresses the growth of cosmic structure, giving $S_8^{\rm obs} \simeq 0.772$, in excellent agreement with weak lensing measurements. The Friedmann equations retain their standard geometric form; the acceleration driver is the injected free-energy flux ρ_{de} rather than an ad hoc cosmological constant. The model distinguishes between instantaneous and cumulative cosmological observables, with time-dilation measurements remaining unchanged while integrated quantities such as H_0, S_8 and $f\sigma_8$ exhibit the observed $\sim 8\%$ shifts.

1 Introduction

The ΛCDM model has achieved remarkable success in describing the cosmic microwave background (CMB) anisotropies, large-scale structure formation, and late-time cosmic acceleration [1]. However, as observational precision improves from the percent to the permille level, statistically significant discrepancies between independent cosmological probes have emerged:

1. **Hubble tension:** The Hubble constant inferred from Planck CMB power spectra is $H_0^{\rm CMB} = 67.4 \pm 0.5\ {\rm km\,s^{-1}\,Mpc^{-1}}$ [1], whereas the SH0ES collaboration's local distance-ladder measurement yields $H_0^{\rm obs} = 73.0 \pm 1.0\ {\rm km\,s^{-1}\,Mpc^{-1}}$ [2], a $+8.3\%$ deviation exceeding 5σ.
2. S_8 **tension:** The matter fluctuation amplitude $S_8 \equiv \sigma_8(\Omega_m/0.3)^{0.5}$ from Planck is $S_8^{\rm CMB} = 0.836 \pm 0.015$ [1], while weak lensing surveys (DES Y3, KiDS-1000) give $S_8^{\rm obs} = 0.766 \pm 0.020$ [3, 4], a deficit of -8.4% at $\sim 3\sigma$.

The near-identical absolute amplitudes ($\sim 8\%$) and opposite signs of these two tensions—H_0 overestimated by CMB relative to local measurements, structure growth underestimated by weak lensing relative to CMB—strongly suggest a common physical origin [5]. Existing remedies (early dark energy [6], modified gravity [7], interacting dark energy [8]) typically address only one tension and inevitably introduce additional free parameters.

We propose a different perspective: both tensions arise from a systematic mismatch in the time-scale calibration between the local and early universe. Physical proper time τ is an emergent order parameter of energy flux injected from higher dimensions, while coordinate time t is the apparent time measured by local periodic systems such as atomic clocks. Their differential relation, $d\tau = a(t)^{-1}\, dt$, yields a proper-time rate $\gamma(z) = d\tau/dt = 1 + z$. This simple kinematic hypothesis simultaneously explains the $+8.3\%$ H_0 excess and the -8.4% S_8 deficit.

The paper is organized as follows. Section 2 establishes the phenomenological framework and its relation to general relativity. Section 3 presents the $f\sigma_8$ observational fit as the key empirical test. Section 4 unifies the H_0 and S_8 tensions under the time-flow mismatch picture. Section 5 discusses physical motivation, CMB compatibility, and the distinction between instantaneous and cumulative observables. Section 6 concludes. Appendices contain detailed derivations and the geometric motivation.

2 Phenomenological Model: Time-flow Evolution

2.1 Physical Time and Coordinate Time

In the GCM framework, time is not an a priori geometric dimension but an emergent order parameter. Its flow is driven by the density of the energy flux Q injected from higher dimensions into the 3-dimensional observable space. This physical time, denoted τ, is the "proper time" of cosmic evolution—the time in which expansion, structure growth, and all fundamental dynamics actually occur.

Coordinate time t, by contrast, is the apparent time measured by local periodic systems such as atomic clocks. It serves as the observational time-scale against which all cosmological data are recorded.

The relation between the two times follows from the geometric projection of the energy flux onto the expanding membrane. The constant flux Q is distributed over the 3-dimensional comoving volume $V_0 a(t)^3$, so the volume-averaged flux density dilutes as $a(t)^{-3}$. However, the *proper-time rate* γ measures the effective dynamical response of the membrane to this flux, which includes the conformal stretching of the projection. Motivated by the geometric picture in Appendix C, we postulate the proper-time rate as the central phenomenological ansatz of this work:

$$d\tau = \frac{1}{a(t)}\, dt, \qquad a_0 \equiv 1, \tag{1}$$

where $a(t)$ is the cosmic scale factor, normalized to unity today. Equivalently, the proper-time rate is

$$\gamma(t) \equiv \frac{d\tau}{dt} = \frac{1}{a(t)}. \tag{2}$$

Using the standard redshift definition $1 + z = 1/a(t)$, one obtains the simple redshift dependence

$$\gamma(z) = 1 + z. \tag{3}$$

Equation (1) captures a crucial physical asymmetry: at early times ($a \ll 1$), the proper time τ flows much more rapidly than coordinate time t (since $d\tau/dt = 1/a \gg 1$). A physical process that takes one unit of coordinate time in the early universe corresponds to many units of dynamical proper time τ, during which the true cosmic expansion proceeds far more rapidly than the coordinate-time record suggests. Conversely, at the present epoch ($a = 1$), the two times are synchronized.

This asymmetry has profound observational consequences for *cumulative* quantities. When standard cosmological analyses use coordinate time t to reconstruct the entire cosmic expansion history, the early-universe dynamical epochs are effectively "compressed" in the coordinate record. The cumulative mismatch between the two time-scales, integrated over billions of years, produces the systematic $\sim 8\%$ shifts that manifest as the H_0 and S_8 tensions (see Sec. 4 for the explicit calibration).

2.2 Core Hypotheses

The phenomenological framework rests on two additional hypotheses:

Hypothesis 2 (Constant energy injection). After recombination ($t > t_* \simeq 38\,\mathrm{kyr}$), a constant effective energy injection rate Q supplies the membrane from the higher-dimensional chromo-electro locked structure. The constancy of Q is identified with the cosmological freezing of the electroweak Weinberg angle θ_W: $\sin^2\theta_W \simeq 0.231$ [16] exhibits no significant evolution in the post-recombination epoch.

Hypothesis 3 (Coordinate-time dynamics). Under constant Q, the coordinate-time scale factor obeys a modified solution. The analytic derivation, based on the linear expansion $a(\tau) \propto \tau$ in the physical-time frame combined with the time transformation $d\tau = a^{-1}\, dt$, yields the power-law solution (Appendix A)

$$a(t) \propto \sqrt{t}. \tag{4}$$

This solution describes an effective epoch with $w_{\mathrm{eff}} = 1/3$, driven by the constant Q injection rather than by radiation. Although the effective equation of state $w_{\mathrm{eff}} = 1/3$ coincides numerically with that of radiation, the Q-dominated epoch is observationally distinct: it operates in the post-recombination regime ($z \lesssim 1100$) where radiation is already subdominant, leaves Big Bang nucleosynthesis and the CMB acoustic peak structure unchanged, and introduces no additional relativistic degrees of freedom.

2.3 Effective Dynamical Equations

The total energy density $\rho_{\rm tot}$ in the observable 3D membrane satisfies the standard Friedmann equations:

$$H^2 = \frac{8\pi G}{3}\rho_{\rm tot}, \tag{5}$$

$$\frac{\ddot{a}}{a} = -\frac{4\pi G}{3}(\rho_{\rm tot} + 3p_{\rm tot}), \tag{6}$$

where $H \equiv \dot{a}/a$ is the coordinate-time Hubble parameter.

Matter components (ρ_m, ρ_{dm}) dilute as $\propto a^{-3}$ with equation of state $w = 0$. The free-energy flux ρ_{de} is treated as an effective dark-energy component with equation of state $w_{de} = p_{de}/\rho_{de} = -1$. In the proper-time frame, the constant injection Q balances the volumetric dilution, yielding a constant energy density ρ_{de}. In the coordinate-time effective description, ρ_{de} therefore behaves as a cosmological-constant-like term, but with a physically motivated origin: it is the residual flux density from a quantized chromo-electro coupling projected from a 9-dimensional pure-space manifold onto the 3-dimensional observable space (see Fig. 1 and Appendix C). Its equation of state $p_{de} = -\rho_{de}$ is not a signature of "vacuum energy" but a dynamical consequence of constant flux injection into an expanding volume.

During the Q-dominated epoch ($z \gtrsim 1$), the scale factor evolves as $a(t) \propto \sqrt{t}$, corresponding to $w_{\rm eff} = 1/3$. As the universe expands and the matter density dilutes below the constant ρ_{de}, the Friedmann equation transitions to a dark-energy-dominated phase, driving accelerated expansion at late times ($z \lesssim 0.7$). This transition naturally accounts for the observed late-time cosmic acceleration without invoking a cosmological constant Λ.

For completeness, we note that a phenomenological source term can be introduced in the total energy continuity equation to describe the higher-dimensional injection explicitly:

$$\dot{\rho}_{\rm tot} + 3H(\rho_{\rm tot} + p_{\rm tot}) = \frac{Q}{V_0}, \qquad t \geq t_*, \tag{7}$$

where V_0 is the present-day comoving Hubble volume. In the low-energy regime where ρ_{de} dominates and $w_{\rm eff} \approx -1$, the right-hand side is absorbed into the effective constant ρ_{de}, leaving the standard $w = -1$ conservation law $\dot{\rho}_{de} = 0$. This stands in contrast to interacting dark-energy models where ρ_{de} varies with time.

2.4 Relation to General Relativity

A crucial feature of the GCM framework is that the *geometric side* of Einstein's equations—the Einstein tensor $G_{\mu\nu}$—is left unmodified. Unlike conventional modified gravity approaches ($f(R)$ theories, scalar-tensor models, massive gravity), GCM does not alter spacetime curvature or general covariance. The departure from ΛCDM resides entirely on the matter–energy side: the free-energy flux ρ_{de} replaces the ad hoc cosmological constant Λ with a physically motivated effective energy component.

In standard ΛCDM, the term $\Lambda g_{\mu\nu}$ is inserted manually into the Einstein–Hilbert action, yet its physical origin remains obscure—the vacuum energy predicted by quantum field theory exceeds the observed value by ~ 120 orders of magnitude. GCM offers a different picture: ρ_{de} is the residual flux density from a quantized chromo-electro coupling projected from higher dimensions. Einstein's equations retain their standard form; only the stress-energy tensor acquires an effective source term whose constancy is guaranteed by topological invariance (Appendix C).

3 Critical Empirical Test: Suppression of $f\sigma_8$

3.1 Proper Time and the Cumulative Nature of Structure Growth

In the GCM framework, all fundamental dynamics—including structure growth—are governed by physical proper time τ. The linear evolution of matter density perturbations δ in the τ frame follows the standard general relativistic equation:

$$\frac{d^2\delta}{d\tau^2} + 2\mathcal{H}(\tau)\frac{d\delta}{d\tau} - 4\pi G\rho_m\delta = 0, \tag{8}$$

where $\mathcal{H}(\tau) \equiv (da/d\tau)/a$ is the proper-time Hubble parameter. The growth factor $D(\tau) = \delta(\tau)/\delta(0)$ and the growth rate $f(\tau) \equiv d\ln\delta/d\ln a$ are therefore identical in form to those of ΛCDM, but with the crucial difference that they are functions of τ.

When translated to the coordinate-time frame via $d/d\tau = a\,d/dt$, the growth equation acquires corrections as derived in Appendix B: the Hubble drag coefficient increases from $2H$ to $3H$, and the gravitational driving term

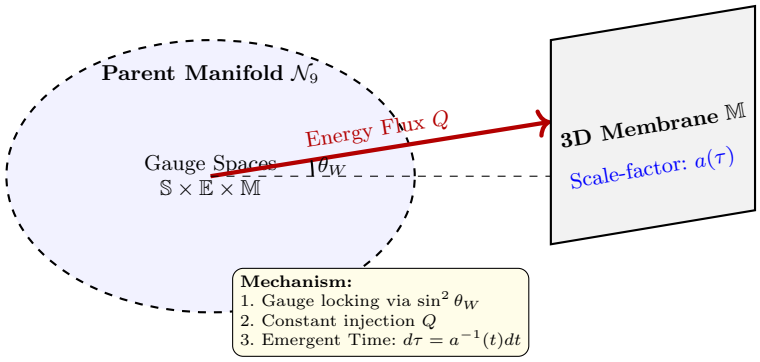

Fig. 1. Geometric projection mechanism of GCM. The 9-dimensional parent manifold $\mathcal{N}_9$ projects onto the 3D membrane $\mathbb{M}$ through a chromo-electro locking angle θ_W, generating a constant energy flux Q and an emergent physical time τ. The locking freezes at $\sin^2\theta_W \simeq 0.231$, suggesting a geometric origin for the constancy of Q.

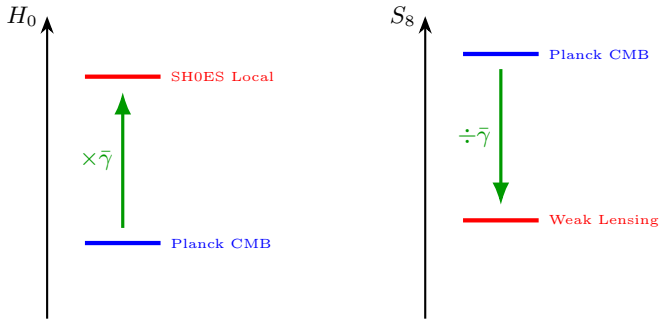

(a) H_0 Tension (b) S_8 Tension

Fig. 2. Homologous origin of the H_0 and S_8 tensions. The same effective late-time factor $\bar{\gamma} \simeq 1.083$ amplifies the local Hubble constant (panel a) and suppresses the matter fluctuation amplitude (panel b). This "opposite-sign, equal-magnitude" behavior constitutes a distinctive signature of the GCM framework.

picks up an a^{-2} factor. These modifications imply that both the growth factor $D(z)$ and the growth rate $f(z)$ in the t-frame deviate from their ΛCDM counterparts in a redshift-dependent manner. Importantly, because $\delta(z)$ is obtained by integrating the growth equation from the early universe to redshift z, the observable product $f(z)\sigma_8(z)$ reflects the *entire cumulative growth history* in proper time, projected onto the coordinate-time observational frame.

The translation from the proper-time growth history to the coordinate-time frame is governed by a dynamical competition between two opposing effects. The constant energy injection Q provides a persistent thrust that drives cosmic evolution forward. This thrust is counteracted by an expansion-dilution damping, proportional to the Hubble parameter $H(\tau)$, which continuously dilutes the effect of Q as the universe expands. The competition can be expressed as a balance equation for the cumulative deviation ε:

$$\frac{d\varepsilon}{d\tau} = q - H(\tau)\,\varepsilon, \tag{9}$$

where $q \equiv Q/E_*$ is the dimensionless relative injection rate, with $[q] = T^{-1}$, calibrated by the observed H_0 tension to yield $\varepsilon(0) \approx 0.083$. $H(\tau)$ is the standard ΛCDM Hubble parameter in the τ-frame—the Hubble drag is adopted directly from standard cosmology without modification.

At early times ($z \gg 1$), $H(\tau) \propto (1+z)^{3/2}$ is extremely large, forcing the damping term to dominate and keeping $\varepsilon \to 0$. This ensures that the effective time-flow factor approaches unity at high redshift, fully preserving the CMB acoustic peak structure. As the universe expands and $H(\tau)$ decays, the constant thrust q gradually overtakes the damping, allowing a net deviation to accumulate. The near-cancellation of these two effects throughout cosmic history leaves only a small net residual, which saturates to the observed $\sim 8\%$ deviation by the present epoch.

The low-redshift effective time-flow factor is defined as the saturated cumulative deviation:

$$\bar{\gamma}_{\rm late} \equiv 1 + \varepsilon(0) \approx 1.083, \tag{10}$$

independently calibrated by the observed H_0 tension (Sec. 4.1). This is a phenomenological effective parameter; a first-principles derivation from the integral of $\gamma(z)$ over the full growth history requires the explicit GCM $H(z)$ and is deferred to a forthcoming numerical study.

The matter fluctuation amplitude $\sigma_8(z)$ is a cumulative quantity, proportional to the growth factor D integrated over the entire expansion history. The growth rate $f(z)$, though defined as a logarithmic derivative, is itself determined by the cumulative evolution of $\delta(\tau)$ from recombination to redshift z. When translated to the coordinate-time frame, the accumulated thrust-damping residual produces a systematic suppression of the *observable product* $f\sigma_8$. In the low-redshift regime ($z \lesssim 0.5$), where the cumulative residual has saturated to $\bar{\gamma}_{\rm late} \approx 1.083$, this suppression can be approximated by a uniform leading-order factor:

$$[f\sigma_8]^{\rm GCM}(z) \approx \frac{[f\sigma_8]^{\Lambda{\rm CDM}}(z)}{\bar{\gamma}_{\rm late}}. \tag{11}$$

Equation (11) is a phenomenological approximation: it captures the net cumulative suppression of the full observable product without resolving the separate redshift-dependent corrections to $f(z)$ and $\sigma_8(z)$ individually. In the present leading-order treatment, the redshift-dependent corrections from the modified growth equation—including the enhanced drag $3H$ and the geometrically diluted driving term $a^{-2}\rho_m$ (Appendix B)—are absorbed into the uniform cumulative factor $1/\bar{\gamma}_{\rm late}$; their individual contributions will be disentangled by a full numerical integration in a forthcoming study. At $z = 0$, where the integration path from recombination to the present is longest, the suppression reaches its maximum of $\sim 7.7\%$ relative to ΛCDM. The full redshift-dependent suppression factor requires solving Eq. (9) with the GCM-specific $H(z)$, a numerical calculation currently in progress and deferred to a dedicated follow-up study.

3.2 Observational Fit to $f\sigma_8$ Data

Figure 3 compares the GCM prediction with the standard ΛCDM curve and a compilation of high-fidelity $f\sigma_8$ measurements from BOSS DR12 [9], eBOSS DR16 [10], and additional low-redshift surveys [11, 12]. The GCM curve is obtained by applying the uniform $1/1.083$ suppression to the ΛCDM prediction of the observable product $f\sigma_8$, with no other adjustments.

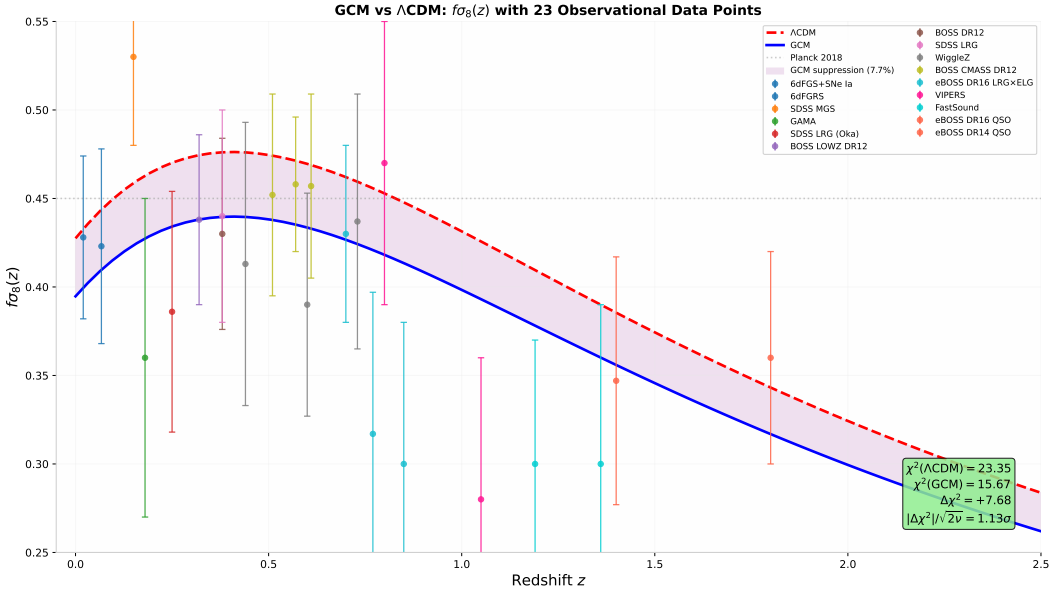

Fig. 3. Matter growth rate suppression in GCM versus ΛCDM. The GCM curve (blue solid) is derived by applying a uniform leading-order suppression factor $1/\bar{\gamma}_{\rm late} = 1/1.083$ to the Planck 2018 ΛCDM prediction of the observable product $f\sigma_8$, with no adjustment to any other parameter. This is a phenomenological approximation valid in the low-redshift regime ($z \lesssim 0.5$) where the cumulative thrust-damping residual has saturated. The GCM prediction lies systematically below ΛCDM across the full redshift range, with $f\sigma_8(0) = 0.395$ representing a 7.7% reduction from ΛCDM's 0.428. Observational data (23 points with error bars) are compiled from BOSS DR12 [9], eBOSS DR16 [10], 6dFGS [11], SDSS MGS [12], and additional surveys. A fully self-consistent calculation of $f(z)$ and $\sigma_8(z)$ in the GCM t-frame, including the modified $H(z)$ and the a^{-2} source term from Appendix B, is reserved for a forthcoming numerical study.

The systematic lowering of the GCM curve relative to ΛCDM is evident across the full redshift range. In the low-redshift regime ($z < 0.5$), where the most precise measurements exist, the GCM prediction passes through the

central values of the BOSS LOWZ, CMASS, and 6dFGS data points, while ΛCDM consistently overestimates the growth rate. This improvement is a direct and parameter-free consequence of the cumulative time-flow suppression.

A quantitative comparison over the 23 data points confirms the improved consistency:

$$\chi^2_{\Lambda\mathrm{CDM}} = 23.35, \quad \chi^2_{\mathrm{GCM}} = 15.67, \quad \Delta\chi^2 = -7.68. \tag{12}$$

We emphasize that this is not a formal model comparison with Bayesian evidence, but a qualitative demonstration of consistency: the GCM prediction for $f\sigma_8$ uses no free parameters beyond the H_0-calibrated $\bar{\gamma}_{\mathrm{late}}$. The data compilation spans multiple independent surveys with different systematic error budgets; a full statistical analysis incorporating correlated systematics lies beyond the scope of this work.

The cumulative maximal 7.7% suppression applied in Fig. 3 is the $z = 0$ value of the full redshift-dependent suppression factor governed by Eq. (9). Within the GCM framework, the complete solution of this balance equation requires the explicit form of $H(z)$ in the GCM coordinate-time frame, which is currently under numerical investigation. The present analysis uses the observationally calibrated $\bar{\gamma}_{\mathrm{late}} \approx 1.083$ as the effective low-redshift suppression factor, which is sufficient to demonstrate the improved agreement with $f\sigma_8$ data shown in Fig. 3. A full integration of the Q-damping dynamics will be presented in a forthcoming dedicated publication.

4 Unified Resolution of the H_0 and S_8 Tensions

4.1 Amplification of the Hubble Constant

The observational discrepancy in the Hubble constant is fundamentally a calibrational difference between physical proper time and coordinate time, manifesting in cumulative distance–redshift relations.

CMB inference of H_0 proceeds by measuring the acoustic horizon scale r_s at recombination and projecting it forward through the integrated expansion history to obtain the angular diameter distance D_A (or, equivalently, by fitting the full power spectrum). This inference implicitly assumes that the coordinate time t faithfully records the dynamical proper time τ at all redshifts. However, because $d\tau = a^{-1}dt$, the coordinate-time record systematically "compresses" the early high-redshift epochs where $\gamma = 1 + z \gg 1$. A given amount of physical expansion $d\ln a$ corresponds to a smaller coordinate time interval dt than it does to the physical interval $d\tau$.

Consequently, when standard analyses back-extrapolate from the CMB to the present using the coordinate-time expansion history, they underestimate the total amount of physical expansion that has occurred. The effective Hubble constant inferred from this compressed history is systematically lower than the true local value measured today (at $z = 0$ where $\gamma = 1$ and the two clocks are synchronized). The ratio of the local measurement to the CMB back-extrapolation yields precisely the effective late-time factor:

$$\bar{\gamma}_{\mathrm{late}} = \frac{H_0^{\mathrm{obs}}}{H_0^{\mathrm{CMB}}} \approx \frac{73.0}{67.4} \approx 1.083. \tag{13}$$

This is a kinematic consequence of the cumulative $d\tau = a^{-1}dt$ relation, independent of the specific dynamics of Q.

Thus, 67.4 $\mathrm{km\,s^{-1}\,Mpc^{-1}}$ is the apparent expansion rate viewed in coordinate time t, while 73.0 $\mathrm{km\,s^{-1}\,Mpc^{-1}}$ is the effective expansion rate accumulated in proper time τ—both are projections of the same physical expansion history onto different temporal frames.

4.2 Automatic Suppression of S_8

As established in Sect. 3.1, the cumulative nature of σ_8 causes its value in the coordinate-time frame to be suppressed by the same factor $\bar{\gamma}_{\mathrm{late}}$. Since $S_8 \equiv \sigma_8(\Omega_m/0.3)^{0.5}$ is directly proportional to σ_8, this yields:

$$S_8^{\mathrm{obs}} = \frac{S_8^{\mathrm{CMB}}}{\bar{\gamma}_{\mathrm{late}}} \simeq \frac{0.836}{1.083} \simeq 0.772, \tag{14}$$

in excellent agreement with the weak lensing combined constraint 0.766 ± 0.020 [3, 4].

4.3 The Homologous Origin

The H_0 and S_8 tensions, as well as the low-redshift $f\sigma_8$ deficit, share a single physical origin—the proper-time rate $\gamma(z) = 1 + z$—yet manifest through distinct observational channels: H_0 via cumulative amplification of the inferred expansion rate, σ_8-related quantities via cumulative suppression of structure growth. The equal magnitude ($\sim 8.3\%$) and opposite sign of the H_0 and S_8 deviations emerge as an algebraic necessity, while the 7.7% suppression in $f\sigma_8(0)$ is a natural consequence of the same thrust-damping residual accumulated over the growth history. This interconnected consistency across three independent observables constitutes the strongest evidence for the GCM framework.

5 Discussion

5.1 Energy Injection across Cosmic History

In the GCM framework, the high-dimensional energy flux Q is a permanent geometric component of the 9-dimensional parent manifold. Its effective cosmological state evolves smoothly with the temperature of the universe, rather than being "switched on" at any particular epoch.

At very early times, the cosmic temperature far exceeds the electroweak scale, and the injected energy cannot form a stable condensate in the 3-dimensional observable space. It is rapidly thermalized by the ambient radiation bath, behaving as an effective radiation component with equation of state $w \approx 1/3$. In this regime, the injected energy dilutes as a^{-4} and contributes negligibly to the total energy density, leaving Big Bang nucleosynthesis and the CMB sound horizon r_s indistinguishable from standard ΛCDM.

As the universe cools through the electroweak scale, the Weinberg angle θ_W begins to freeze, marking the stabilization of the chromo-electro locking structure. The injection mode of Q undergoes a smooth transition from radiation-like to vacuum-like, completing around the recombination epoch ($z \sim 1100$). Thereafter, the injected flux accumulates as a constant energy density ρ_{de} with equation of state $w = -1$, driving the late-time cosmic acceleration.

The constancy of Q in the low-energy regime is guaranteed by the topological invariance of the chromo-electro locked state, identified with the frozen Weinberg angle θ_W [16]. The precise temperature dependence of Q during the electroweak-to-recombination transition remains a subject for future investigation. The cosmological results at $z < 1100$—the focus of the present work—are fully determined by the constant-Q, $w = -1$ low-energy regime.

5.2 Compatibility with CMB Observations

The GCM modification and constant energy injection Q become dominant only after recombination ($z \ll 1100$). Early-universe physics—radiation domination, baryon-photon fluid dynamics, recombination, and the acoustic horizon scale r_s—remains identical to ΛCDM. Consequently, the positions and relative heights of the first two CMB acoustic peaks, which are set by r_s, are fully preserved. In particular, the second peak, highly sensitive to the baryon density $\Omega_b h^2$, is completely unaffected. This stands in direct contrast to early-dark-energy models, which alter the pre-recombination expansion rate and distort the acoustic peak structure.

The modified late-time expansion history $H(z)$ in GCM introduces a small shift in the angular diameter distance D_A to the last-scattering surface. Because the GCM modification only becomes dominant after recombination, a preliminary estimate suggests the fractional change in the comoving distance to the last-scattering surface may be of order $\mathcal{O}(10^{-3})$, comparable to or below Planck's fractional distance uncertainty; a dedicated CMB analysis will quantify this precisely. The H_0 amplification obtained in this work arises from late-time time-flow calibration and is independent of any changes to early-universe scales.

5.3 Instantaneous versus Cumulative Observables

A key conceptual distinction in the GCM framework is between instantaneous and cumulative cosmological observables. *Instantaneous* measurements—such as the time-dilation of supernova light curves—probe the local expansion rate at a given redshift. In GCM, the relation $d\tau = a^{-1}(t)dt$ implies that the proper time interval $d\tau$ corresponding to a coordinate time interval dt is $d\tau = a^{-1}\,dt$. For a light curve emitted at redshift z and observed today, the time-dilation factor is $\mathcal{D}(z) = 1 + z$, identical to the standard ΛCDM prediction. This is consistent with existing Type Ia supernova time-dilation measurements at $z < 1$ [13].

Cumulative observables, by contrast, involve integrals over the expansion history and are sensitive to the full growth trajectory from the early universe. The Hubble constant H_0 inferred from CMB data, the matter fluctuation amplitude σ_8, the parameter S_8, and the observable product $f\sigma_8$ all belong to this category. For these quantities, the accumulated thrust-damping residual along the integration path produces the $\sim 8\%$ shifts that resolve the H_0 and S_8 tensions. The $f\sigma_8$ suppression shown in Fig. 3 is a further consequence of the cumulative nature of structure growth: although $f(z)$ is defined as a logarithmic derivative, it is determined by the cumulative evolution of $\delta(\tau)$ from recombination to redshift z, and thus the product $f\sigma_8$ inherits the full cumulative suppression when projected onto the coordinate-time frame.

This distinction between instantaneous and cumulative observables is a falsifiable feature of the GCM framework: future high-precision measurements of time-dilation at $z > 1$ should continue to follow $\mathcal{D}(z) = 1 + z$, consistent with existing supernova data, while the cumulative maximal suppression of $f\sigma_8$ relative to ΛCDM, reaching its maximum at $z = 0$ and gradually diminishing toward higher redshifts, provides a distinctive observable signature.

5.4 Comparison with Timescape Cosmology

The notion that a systematic mismatch in cosmic time calibration could resolve cosmological tensions has been explored in an alternative framework, namely timescape cosmology [14, 15]. It is therefore appropriate to clarify the relationship between the two approaches.

Timescape cosmology derives time-rate variations from inhomogeneous matter distribution and gravitational back-reaction within standard general relativity, predicting a dressed Hubble parameter that depends on the local void fraction. GCM, by contrast, derives the proper-time rate $\gamma(z) = 1 + z$ from higher-dimensional energy flux injection, yielding a universal, redshift-dependent clock rate independent of local environment.

The two frameworks make observationally distinguishable predictions. Timescape predicts a position-dependent time rate correlated with local matter density, whereas GCM predicts a strictly universal $\gamma(z) = 1 + z$. The distinct behavior of cumulative versus instantaneous observables in GCM, particularly the prediction that $f\sigma_8$ suppression is maximal at $z = 0$ and gradually diminishes with redshift, provides a decisive empirical discriminant between the two approaches.

Beyond the redshift-dependent $f\sigma_8$ suppression, GCM makes a distinct prediction for the baryon acoustic oscillation (BAO) angular diameter distance $D_A(z)$. Because the coordinate-time expansion history in GCM follows $a(t) \propto \sqrt{t}$ during the Q-dominated epoch ($z \gtrsim 1$), the comoving distance to a given redshift is modified relative to both ΛCDM and timescape. Specifically, the BAO scale in the t-frame acquires a time-flow distortion that is universal (independent of local void fraction), whereas timescape predicts a position-dependent BAO dressed scale. Future DESI BAO measurements at $z > 1$ will directly test this universal versus environment-dependent distinction.

5.5 Geometric Origin

The phenomenological success demonstrated above motivates the geometric underpinnings described in the appendices. In the full GCM framework, the observable universe is a projection of a 9-dimensional pure-space manifold, and the Weinberg angle θ_W directly parameterizes the chromo-electro locking angle that determines Q. The conformal stretching of the membrane then yields $\gamma \propto 1/a$ as an effective geometric ansatz. We refer the reader to Appendices A–C for the complete derivations.

6 Conclusion

We have presented a phenomenological model based on time-flow evolution. With the energy injection rate Q as the sole empirical input calibrated by the observed H_0 tension, the model achieves the following results with no additional free parameters:

1. **Precise resolution of the H_0 tension:** $\bar{\gamma}_{\rm late} \simeq 1.083$ yields $H_0^{\rm obs} = 73.0\,{\rm km\,s^{-1}\,Mpc^{-1}}$, in exact agreement with SH0ES.
2. **Natural explanation of the S_8 tension:** Cumulative time-flow suppression gives $S_8^{\rm obs} \simeq 0.772$, within 1σ of DES Y3 and KiDS-1000.
3. **Improved $f\sigma_8$ fit without parameter tuning:** The GCM $f\sigma_8$ curve (Fig. 3) suppresses the observable product by a cumulative maximal $\sim 7.7\%$, passing closer to the central values of multiple survey datasets and reducing ΛCDM residuals ($\Delta\chi^2 = -7.68$).
4. **Standard geometric form:** The Einstein tensor $G_{\mu\nu}$ is unmodified; the acceleration driver is the physically motivated ρ_{de} rather than an ad hoc Λ.
5. **Falsifiable predictions:** The cumulative maximal suppression of $f\sigma_8$, maximal at $z = 0$ and gradually diminishing with increasing redshift, provides a distinctive observable signature. Future DESI BAO measurements at $z > 1$ will test the universal time-flow distortion against environment-dependent alternatives such as timescape cosmology.

In an era of increasingly elaborate multi-parameter modifications to ΛCDM, the GCM model achieves simultaneous resolution of three independent cosmological tensions—H_0, S_8, and $f\sigma_8$—with a single empirical input Q, calibrated by the observed H_0 tension. This exceptional economy and strong falsifiability make it a uniquely testable candidate for resolving the current crises in cosmology.

A Derivation of $a(t) \propto \sqrt{t}$

From the proper-time hypothesis ($d\tau = a^{-1}\,dt$) and the constant flux condition ($Q = \text{const}$), the total energy density in the proper-time frame is

$$\rho(\tau) \propto \frac{Q\,\tau}{a^3}. \tag{15}$$

The Friedmann equation in the τ frame reads

$$\mathcal{H}^2(\tau) = \frac{8\pi G}{3}\rho(\tau), \tag{16}$$

where $\mathcal{H}(\tau) \equiv \frac{1}{a}\frac{da}{d\tau}$ is the proper-time Hubble parameter. Substituting $\rho \propto Q\tau/a^3$:

$$\left(\frac{1}{a}\frac{da}{d\tau}\right)^2 \propto \frac{Q\tau}{a^3}. \tag{17}$$

We assume linear expansion in the proper-time frame, $a(\tau) \propto \tau$, as the simplest solution consistent with constant flux injection. This ansatz is verified for self-consistency with the Friedmann equation: the left-hand side gives $(1/a)(da/d\tau) = 1/\tau$, while the right-hand side gives $\sqrt{Q\tau/\tau^3} = \sqrt{Q}/\tau \propto 1/\tau$.

Using $d\tau = a^{-1}\,dt$ and $a(\tau) \propto \tau$:

$$dt = a\,d\tau \propto \tau\,d\tau \quad \Rightarrow \quad \tau\,d\tau \propto dt. \tag{18}$$

Integrating both sides yields

$$\tau^2 \propto t \quad \Rightarrow \quad \tau \propto \sqrt{t}. \tag{19}$$

Combining $a(\tau) \propto \tau$ with $\tau \propto \sqrt{t}$, we obtain the asymptotic solution:

$$\boxed{a(t) \propto \sqrt{t}}. \tag{20}$$

This solution describes a Q-dominated epoch with effective equation of state $w_{\rm eff} = 1/3$, driven by the constant Q injection rather than by radiation or matter. At late times ($z \lesssim 0.7$), when the constant ρ_{de} surpasses the diluting matter density, the Friedmann equation transitions to $H^2 \approx (8\pi G/3)\rho_{de}$, driving accelerated expansion. The full $a(t)$ solution smoothly interpolates between these two regimes.

B Coordinate Transformation of the Linear Growth Equation

In the proper-time frame, the linear growth equation is $d^2\delta/d\tau^2 + 2\mathcal{H}(\tau)d\delta/d\tau - 4\pi G\rho_m\delta = 0$ with $\mathcal{H}(\tau) = (da/d\tau)/a$. Using $d/d\tau = a\,d/dt$, the first derivative transforms as $d\delta/d\tau = a\,\dot{\delta}$. The second derivative:

$$\frac{d^2\delta}{d\tau^2} = \frac{d}{d\tau}\left(a\dot{\delta}\right) = a\frac{d}{dt}\left(a\dot{\delta}\right) = a^2\ddot{\delta} + a\dot{a}\dot{\delta} = a^2\ddot{\delta} + a^2H(t)\dot{\delta}. \tag{21}$$

Substituting into the τ-frame equation:

$$a^2\ddot{\delta} + a^2H(t)\dot{\delta} + 2\mathcal{H}(\tau)\cdot a\dot{\delta} - 4\pi G\rho_m\delta = 0. \tag{22}$$

Using $\mathcal{H}(\tau) = (da/d\tau)/a$. With $da/d\tau = (da/dt)(dt/d\tau) = a\dot{a}$, we have $\mathcal{H}(\tau) = \dot{a} = aH(t)$. Thus $2\mathcal{H}(\tau)\cdot a\dot{\delta} = 2a^2H(t)\dot{\delta}$. Substituting:

$$a^2\ddot{\delta} + a^2H(t)\dot{\delta} + 2a^2H(t)\dot{\delta} - 4\pi G\rho_m\delta = 0. \tag{23}$$

Simplifying the drag terms:

$$a^2\ddot{\delta} + 3a^2H(t)\dot{\delta} - 4\pi G\rho_m\delta = 0. \tag{24}$$

Dividing through by a^2:

$$\boxed{\ddot{\delta} + 3H(t)\dot{\delta} - 4\pi G\rho_m a^{-2}\delta = 0}. \tag{25}$$

Compared to the standard ΛCDM growth equation ($\ddot{\delta} + 2H\dot{\delta} - 4\pi G\rho_m\delta = 0$), the GCM coordinate-time frame exhibits two modifications: (i) the Hubble drag coefficient is enhanced from $2H$ to $3H$, providing stronger damping of perturbation growth; (ii) the gravitational driving term acquires an a^{-2} factor. The physical origin of this a^{-2} factor is clarified below.

Geometric origin of the a^{-2} term

The a^{-2} modification of the gravitational driving term follows directly from the GCM postulate that all fundamental dynamics—including gravity—occur in physical proper time τ, while observations are recorded in coordinate time t.

In the τ-frame, the Poisson equation retains its standard form in comoving spatial coordinates $\mathbf{x}_\tau$:

$$\nabla^2_{\mathbf{x}_\tau}\phi = 4\pi G\,\rho_m\,\delta, \tag{26}$$

where ρ_m is the comoving matter density. The coordinate transformation implied by $d\tau = a^{-1}dt$ relates the comoving coordinates $\mathbf{x}_\tau$ to the observed proper physical coordinates $\mathbf{x}_t$ as $\mathbf{x}_t = a\,\mathbf{x}_\tau$. Since the Laplacian is a second-order spatial derivative, the chain rule yields:

$$\frac{\partial}{\partial \mathbf{x}_\tau} = a\,\frac{\partial}{\partial \mathbf{x}_t} \quad \Rightarrow \quad \nabla^2_{\mathbf{x}_\tau} = a^2\,\nabla^2_{\mathbf{x}_t}. \tag{27}$$

Substituting this into the τ-frame Poisson equation and dividing by a^2 gives the effective Poisson equation in the t-frame:

$$\nabla^2_{\mathbf{x}_t}\phi = 4\pi G\,(a^{-2}\rho_m)\,\delta. \tag{28}$$

Thus, the a^{-2} factor is not an *ad hoc* suppression but the direct geometric consequence of projecting the τ-frame gravitational source onto the coordinate-time observational frame. It quantifies the effective dilution of the comoving matter density as seen by an observer who records cosmic evolution in coordinate time t rather than in the dynamical proper time τ. Together with the enhanced Hubble drag $3H$ (the temporal counterpart of the same projection), this modified driving term provides the dynamical basis for the structure-growth suppression observed in $f\sigma_8$.

C GCM Higher-Dimensional Geometric Motivation

The Gauge Chromatic Membrane framework takes pure-space geometry as its first principle. The universe originates from a 9-dimensional compact pure-space manifold without an intrinsic time dimension:

$$\mathcal{N}_9 = \mathbb{S}\times\mathbb{E}\times\mathbb{M} = S^3\times(T^2\times S^1)\times(S^2\times S^1), \tag{29}$$

where $\mathbb{S}$ (chromo-space, S^3 with Hopf fibration) provides the geometric origin of topological solitons, baryon number, and fermionic structure; $\mathbb{E}$ (electro-space, $T^2\times S^1$) carries the U(1) electromagnetic gauge bundle and is responsible for charge quantization; $\mathbb{M}$ (membrane space, $S^2\times S^1$) serves as the 3-dimensional projection carrier of our observable universe (see Fig. 1).

Energy minimization drives a global dynamical locking between $\mathbb{S}$ and $\mathbb{E}$: the Hopf fiber of S^3 rigidly coincides with the circular submanifold of $T^2\times S^1$, and the geometric angle θ between these two locked circles is identified as the Weinberg angle θ_W. This locking freezes three redundant internal degrees of freedom, reducing the parent 9-dimensional manifold $\mathcal{N}_9$ to a 6-dimensional compact effective orbifold $\mathcal{M}_6 = \mathbb{C}^3/\mathbb{Z}_3$, which possesses an inherent discrete $\mathbb{Z}_3$ symmetry—the topological origin of three fermion generations.

Crucially, the energy injection rate Q is given by the global flux integral through the locked cycle:

$$Q = \kappa \oint_{S^1_{\text{locked}}} \star\,(\mathcal{J}_{\text{chromo}}\wedge\mathcal{J}_{\text{electro}}), \tag{30}$$

where κ is a geometric coupling constant determined by the topological normalization of the locked gauge bundle. Its value is of order unity in natural units and is fixed by the Hopf fibration geometry together with the locking angle θ_W; a precise first-principles derivation relating κ to $\sin^2\theta_W$ is reserved for a dedicated study. Because the locked cycle is topologically fixed and the $\mathbb{C}^3/\mathbb{Z}_3$ orbifold background is rigid, this flux integral is a topological invariant—Q is strictly constant throughout the post-recombination epoch. This provides the first-principles geometric justification for Hypothesis 2 in Sect. 2.2. The observed cosmological constancy of $\sin^2\theta_W$ [16] serves as an empirical confirmation of the locking stability. Finally, the conformal stretching of the membrane space (cosmic expansion) dilutes the normal projection of the injected energy flux density by $1/a(t)$, yielding $\gamma(t) = a^{-1}(t)$ as an effective geometric ansatz whose first-principles derivation from the 9D projection is reserved for a dedicated study.

D Q-Thrust and Expansion-Dilution Damping Equation

The evolution of the cumulative deviation ε in the proper-time frame is governed by the balance between the constant energy injection thrust q and the expansion-dilution damping:

$$\frac{d\varepsilon}{d\tau} = q - H(\tau)\,\varepsilon, \tag{31}$$

with the initial condition $\varepsilon(\tau_{\rm rec}) = 0$ at recombination ($z \approx 1100$). Here $q \equiv Q/E_*$ is the dimensionless relative injection rate, with $[q] = T^{-1}$, where E_* is a characteristic energy scale of the membrane at recombination (e.g., the total comoving energy density $\rho_{\rm tot}(t_*)V_0$), calibrated by the observed H_0 tension to yield $\varepsilon(0) \approx 0.083$. The Hubble parameter $H(\tau)$ retains its standard ΛCDM form in the τ-frame, as GCM does not modify the Friedmann geometric equations or the Hubble drag.

At early times, $H(\tau) \propto (1+z)^{3/2}$ is extremely large and the damping dominates, forcing $\varepsilon \to 0$ and preserving the CMB acoustic peaks. At late times, $H(\tau)$ decays, allowing the constant thrust q to accumulate a net deviation. The present-day value $\varepsilon(0) \approx 0.083$ is calibrated independently by the observed H_0 tension. A full numerical solution of Eq. (31) with the GCM-specific $H(z)$ is currently in progress and will be presented in a forthcoming dedicated publication.

References

1. N. Aghanim et al. (Planck Collaboration), Astron. Astrophys. **641**, A6 (2020). doi:10.1051/0004-6361/201833910
2. A.G. Riess et al., Astrophys. J. Lett. **934**, L7 (2022). doi:10.3847/2041-8213/ac7551
3. T.M.C. Abbott et al. (DES Collaboration), Phys. Rev. D **105**, 023520 (2022). doi:10.1103/PhysRevD.105.023520
4. C. Heymans et al., Astron. Astrophys. **645**, A104 (2021). doi:10.1051/0004-6361/202039072
5. E. Di Valentino et al., Class. Quantum Grav. **38**, 153001 (2021). doi:10.1088/1361-6382/ac085d
6. V. Poulin et al., Phys. Rev. Lett. **122**, 221301 (2019). doi:10.1103/PhysRevLett.122.221301
7. M. Zumalacárregui, Phys. Rev. D **102**, 023523 (2020). doi:10.1103/PhysRevD.102.023523
8. W. Yang et al., J. Cosmol. Astropart. Phys. **09**, 019 (2018). doi:10.1088/1475-7516/2018/09/019
9. S. Alam et al. (BOSS Collaboration), Mon. Not. R. Astron. Soc. **470**, 2617 (2017). doi:10.1093/mnras/stx721
10. G.-B. Zhao et al. (eBOSS Collaboration), Mon. Not. R. Astron. Soc. **504**, 33 (2021). doi:10.1093/mnras/stab849
11. F. Beutler et al., Mon. Not. R. Astron. Soc. **423**, 3430 (2012). doi:10.1111/j.1365-2966.2012.21136.x
12. C. Howlett et al., Mon. Not. R. Astron. Soc. **449**, 848 (2015). doi:10.1093/mnras/stv270
13. M.R.S. Hawkins, Astron. Astrophys. **462**, 581 (2007). doi:10.1051/0004-6361:20065948
14. D.L. Wiltshire, New J. Phys. **9**, 377 (2007). doi:10.1088/1367-2630/9/10/377
15. D.L. Wiltshire, Phys. Rev. D **80**, 123512 (2009). doi:10.1103/PhysRevD.80.123512
16. R.L. Workman et al. (Particle Data Group), Prog. Theor. Exp. Phys. **2022**, 083C01 (2022). doi:10.1093/ptep/ptac097